

ORIGINAL RESEARCH

Open Access



Preclinical evaluation of [^{18}F]SYN1 and [^{18}F]SYN2, novel radiotracers for PET myocardial perfusion imaging

Seweryn Krajewski^{1*} , Lukasz Steczek¹, Karina Gotowicz^{1,2}, Urszula Karczmarczyk³, Joanna Towpik¹, Ewa Witkowska-Patena^{4,5}, Krzysztof Łyczko⁶, Maciej Mazur², Przemysław Kozanecki¹, Joanna Włostowska¹, Juhani Knuti^{7,8}, Mirosław Dziuk^{4,5}, Piotr Garnuszek³ and Cezary Kozanecki¹

Abstract

Background Positron emission tomography (PET) is now an established diagnostic method for myocardial perfusion imaging (MPI) in coronary artery disease, which is the main cause of death globally. The available tracers show several limitations, therefore, the ^{18}F -labelled tracer is in high demand nowadays. The preclinical studies on normal Wistar rats aimed to characterise two potential, novel radiotracers, [^{18}F]SYN1 and [^{18}F]SYN2, to evaluate which is a better candidate for PET MPI radiotracer.

Results The dynamic microPET images showed rapid myocardial uptake for both tracers. However, the uptake was higher and also stable for [^{18}F]SYN2, with an average standardized uptake value of 3.8. The biodistribution studies confirmed that [^{18}F]SYN2 uptake in the cardiac muscle was high and stable (3.02%ID/g at 15 min and 2.79%ID/g at 6 h) compared to [^{18}F]SYN1 (1.84%ID/g at 15 min and 0.32%ID/g at 6 h). The critical organs determined in dosimetry studies were the small intestine and the kidneys. The estimated effective dose for humans was 0.00714 mSv/MBq for [^{18}F]SYN1 and 0.0109 mSv/MBq for [^{18}F]SYN2. The tested dose level of 2 mg/kg was considered to be the No Observed Adverse Effect Level (NOAEL) for both candidates. The better results were achieved for [^{18}F]SYN2, therefore, further preclinical studies were conducted only for this tracer. Radioligand binding assays showed significant responses in 3 from 68 assays: muscarinic acetylcholine M_1 and M_2 receptors and potassium channel hERG. The compound was mostly metabolised via an oxidative N-dealkylation, while the fluor substituent was not separated from the molecule.

Conclusion [^{18}F]SYN2 showed a favourable pharmacodynamic and pharmacokinetic profile, which enabled a clear visualization of the heart in microPET. The compound was well-tolerated in studies in normal rats with moderate radiation exposure. The results encourage further exploration of [^{18}F]SYN2 in clinical studies.

Keywords Radiotracer, Dosimetry, Fluorine-18, PET MPI, Preclinical studies

*Correspondence:

Seweryn Krajewski
skrajewski@synektik.com.pl

¹Research & Development Centre, Synektik SA, Warsaw, Poland

²Department of Chemistry, University of Warsaw, Warsaw, Poland

³Radioisotope Centre POLATOM, National Centre for Nuclear Research, Otwock, Poland

⁴Nuclear Medicine Department, Military Institute of Medicine - National Research Institute, Warsaw, Poland

⁵Affidea Poland, Warsaw, Poland

⁶Institute of Nuclear Chemistry and Technology, Warsaw, Poland

⁷Turku PET Centre, Turku University Hospital and University of Turku, Turku, Finland

⁸Department of Clinical Physiology, Nuclear Medicine, and PET, Turku University Hospital, Turku, Finland



© The Author(s) 2024. **Open Access** This article is licensed under a Creative Commons Attribution 4.0 International License, which permits use, sharing, adaptation, distribution and reproduction in any medium or format, as long as you give appropriate credit to the original author(s) and the source, provide a link to the Creative Commons licence, and indicate if changes were made. The images or other third party material in this article are included in the article's Creative Commons licence, unless indicated otherwise in a credit line to the material. If material is not included in the article's Creative Commons licence and your intended use is not permitted by statutory regulation or exceeds the permitted use, you will need to obtain permission directly from the copyright holder. To view a copy of this licence, visit <http://creativecommons.org/licenses/by/4.0/>.

Background

Ischemic heart disease is a common clinical problem and accurate diagnostic tools are warranted. Among others, nuclear cardiac imaging techniques such as single photon emission computed tomography (SPECT) and positron emission tomography (PET) have been used to detect myocardial ischemia and guiding therapy options such as revascularization [1–4].

The current limiting factor of PET myocardial perfusion imaging (MPI) is availability of tracers, especially in clinical sites without cyclotron [5, 6]. Based on technical superiority of PET over SPECT for myocardial perfusion imaging and feasibility for quantitation of myocardial blood flow in absolute terms [7, 8], the development of new radiotracers for PET MPI may lead to wider use of PET diagnostic imaging in cardiology.

[⁸²Rb]Rubidium chloride ([⁸²Rb]RbCl) is currently the most commonly used tracer for PET MPI, especially in the USA, but is also registered in some countries of the European Union (Luxembourg, Denmark) [9]. The use of [⁸²Rb]RbCl requires a specific generator, which is costly, especially in sites with small number of patients per day. The other PET MPI tracers, [¹³N]ammonia ([¹³N]NH₃) and [¹⁵O]H₂O require on site cyclotron for their production.

The studies on novel PET MPI tracers mainly focus on ¹⁸F-labelled molecules. ¹⁸F seems to be an optimal radioisotope for labelling - its chemistry has been well-studied, it can be easily produced in cyclotrons and transported over considerable distances due to its relatively long half-life.

At present, there are several ¹⁸F-tracers under development, but none of them is currently commercially available [10–12]. One of them, [¹⁸F]flurpiridaz, completed a phase 3 clinical trials showing greater diagnostic accuracy with PET as compared to SPECT MPI [13]. The comparison of available MPI tracers is shown in Table 1.

Myocardial uptake of a tracer depends both on its transport into the cell and its subsequent extraction/retention in the cell. The first process depends on the blood flow and the latter on cell membrane integrity and

viability. The ideal myocardial perfusion agent should have high first-pass extraction fraction and retention by the myocytes, rapid clearance from blood, low extracardiac uptake, minimal myocardial redistribution, intrinsic chemical stability, and relatively simple radiochemical synthesis and purification process [20]. In addition, the extraction fraction should not be substantially influenced by level of flow as this characteristic makes quantitation of myocardial perfusion more feasible.

There is a group of compounds, widely tested on animals, that show these features – ¹⁸F-labelled derivatives of triphenylphosphonium cation with a symmetrical structure [10]. Other compounds, which were promising in MPI in clinical studies, are ¹⁸F-labelled dyes such as rhodamine B and boron-dipyrromethene (BODIPY) derivatives [12, 21]. Taking into account the collected data and that [¹³N]ammonia is an excellent PET MPI tracer, we concluded that desired active pharmaceutical ingredient (API) structure should consist of a nitrogen cationic centre, at least three aromatic rings and be structurally similar to well-known dyes used in staining cell material and organelles. The quaternary ammonium salts, whose main core consists of three fused aromatic rings, commonly used in molecular biology, are ethidium bromide (EthBr) and N-nonyl acridine orange (NOA). We have chosen these compounds as model molecules for developing a novel PET MPI tracer. The EthBr is used to stain the nucleic acids by intercalation between adjacent base pairs. The NOA specifically incorporates into the mitochondrial membrane through primary binding to cardiolipin, a phospholipid present only in the inner layer of the cell membrane [22].

We developed and investigated [¹⁸F]SYN1 and [¹⁸F]SYN2, which are ¹⁸F-labelled derivatives of EthBr and NOA, respectively.

Methods

The presented preclinical studies were conducted using radioactive tracers [¹⁸F]SYN1 and [¹⁸F]SYN2, and also their non-radioactive reference standards (when a high

Table 1 Comparison of available SPECT and PET tracers for myocardial perfusion

	Compound name	Effective dose [14–16] [mSv/MBq]	Recommended dose [17, 18] [MBq]	Sensitivity [13, 19] [%]	Specificity [13, 19] [%]
SPECT	[²⁰¹ Tl]Thallium chloride	0.14	37–111	85	80
	[^{99m} Tc]Tc-sestamibi	0.0079	150–1200	84	76
	[^{99m} Tc]Tc-tetrofosmin	0.0069	150–1200	76	80
PET	[⁸² Rb]Rubidium chloride	0.0011	740–1480	87	84
	[¹³ N]Ammonia	0.002	400	83	91
	[¹⁵ O]H ₂ O	0.0011	400	84	81
	[¹⁸ F]Flurpiridaz	0.015	90–350	80	64

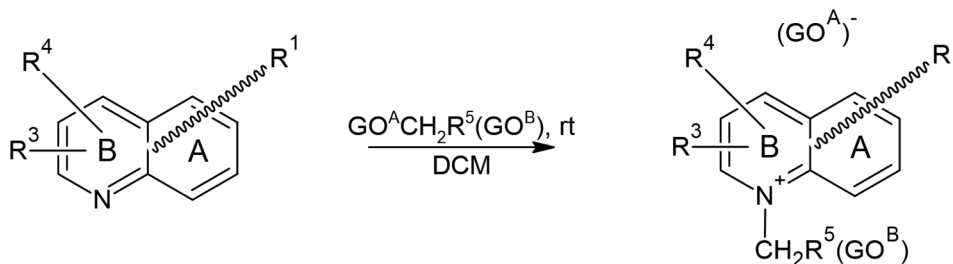


Fig. 1 Precursors synthesis scheme

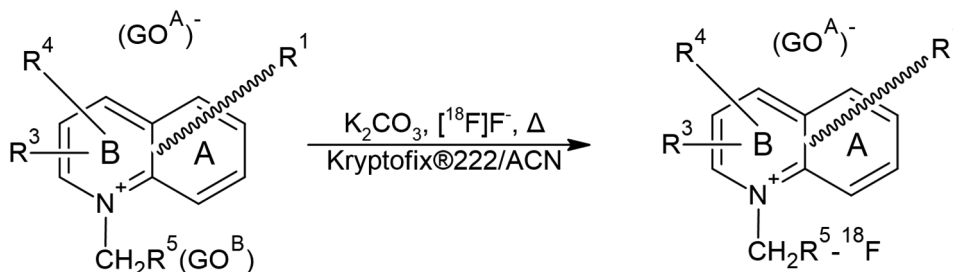


Fig. 2 Radiosynthesis of $[^{18}\text{F}]\text{SYN1}$ and $[^{18}\text{F}]\text{SYN2}$

concentration of the compound was needed to carry out the tests).

Precursor synthesis

The precursors of $[^{18}\text{F}]\text{SYN1}$ and $[^{18}\text{F}]\text{SYN2}$ were synthesized by the method illustrated in Fig. 1. The reagent bearing two groups suitable in a nucleophilic substitution reaction was dissolved in dichloromethane (DCM) and cooled. The phenanthridine derivative or acridine derivative was also dissolved in DCM and added dropwise to the reagent. The contents of the reaction flask were stirred for a given time, and at the end of the reaction, cold Et_2O was added. The precipitate formed was filtered off under reduced pressure. The details are given in patent EP 3 814 325 B1 [23].

Radiosynthesis

The radiosynthesis of $[^{18}\text{F}]\text{SYN1}$ and $[^{18}\text{F}]\text{SYN2}$ is based on $\text{S}_{\text{N}}2$ substitution reaction of $[^{18}\text{F}]\text{F}^-$ with the precursor described above (Fig. 2). The process was carried out using a radiosynthesis module (Modular-Lab Standard, Eckert&Ziegler, Germany). The $[^{18}\text{F}]\text{F}^-$ was produced using the Eclipse HP cyclotron (11 MeV, Siemens, USA). The usual irradiation conditions were a proton current of 60 μA . The produced $[^{18}\text{F}]\text{F}^-$ was captured on the Waters, QMA light SPE column and eluted by a solution of phase-transfer catalyst (Kryptofix[®] 2.2.2., K_2CO_3 , water, acetonitrile) into the reactor. Afterwards, the water/acetonitrile mixture was removed under reduced pressure, and azeotropic distillation was carried out. The precursor solution was added to the dried complex of $[^{18}\text{F}]\text{F}^-$ with phase-transfer catalyst ($[(\text{Kryptofix}^{\circ} 2.2.2.)\text{K}]^+$), and the

mixture was heated. The crude product was diluted with water/ethanol and purified on a semipreparative HPLC column, where the mobile phase was acetate buffer with the addition of ethanol. The product solution was formulated by dilution with saline to a suitable radioactive concentration and then sterilized by filtration.

Quality control

The final product was analysed by HPLC to confirm identity and determine radiochemical purity: Xterra, C18 250 \times 4.6 mm column (Waters) was used with a flow rate 1 mL/min, gradient elution (phase A – water+0.05% TFA, phase B – acetonitrile), UV detection at 270 and 500 nm, and on-line radiometric detection; sample volume: 20 μL . Analysis time was ca. 30 min. The free $[^{18}\text{F}]\text{fluoride}$ amount was determined by TLC using silica gel on aluminium plates and 95% ACN/0.9% saline (V:V; 1:1) as mobile phase. GC method was used to determine the ethanol and residual solvents amount using HP-Fast Residual Solvent column (30 m \times 0.53 mm, 1.00 μm , Agilent).

The formulation stability was tested for 8 h.

Animals

All animal procedures were conducted according to the National Legislation and the Council Directive of the European Communities on the Protection of Animals Used for Experimental and Other Scientific Purposes (2010/63/UE) and the “ARRIVE guidelines for reporting animal research” [24].

Wistar rats (6–7 weeks old) were purchased from the M. Mossakowski Institute of Experimental and

Clinical Medicine, Polish Academy of Sciences in Warsaw (Poland) (microPET and biodistribution studies), Experimental Medicine Centre at the Medical University in Białystok, Poland (toxicity study) or Envigo RMS Spain S.L. (pharmacokinetics study). On arrival, rats were quarantined and observed for at least five days in groups of not more than five in standard cages in the animal facility of the site conducting study. They were housed in a quiet room under constant conditions (22 ± 2 °C, $55 \pm 10\%$ HR, 12 h light/dark cycles) with free access to standard food and water. Veterinarian staff and investigators observed the rats daily to ensure animal welfare and determine if humane endpoints were reached (e.g. hunched and ruffled appearance, apathy, ulceration, severe weight loss).

For the preclinical studies, the animals were randomized into groups containing from 3 to 10 rats per group and time point, depending on the experiment.

MicroPET

The utility of [^{18}F]SYN1 and [^{18}F]SYN2 as heart-targeted tracers was tested in male rats using microPET/CT. The scans were performed on a trimodal small animal scanner Albira Si PET/SPECT/CT Preclinical Imaging System (Bruker, Billerica, MA, USA) in a group of Wistar rats anesthetized with isoflurane (induction 4%, maintenance 1.5–2%). Dynamic PET acquisition started at the time of radiotracer injection via the tail vein ([^{18}F]SYN1 11.7 ± 0.5 MBq and [^{18}F]SYN2 9.6 ± 0.2 MBq) and lasted for 45 min with time frames of 10×30 s, 5×60 s, 5×120 s and 5×300 s.

Biodistribution and pharmacokinetics

The physiological distribution and pharmacokinetics for [^{18}F]SYN1 and [^{18}F]SYN2 were examined on rats according to approved protocol. Approximately 0.2 mL/31.1 MBq of compound was administered i.v. At established time points after injection (15 min, 30 min, 1 h, 2 h, 4 h and 6 h), the animals were euthanized by cervical dislocation and dissected. Selected organs and tissues were weighed, and their radioactivity was measured using a NaI(Tl) crystal gamma counter. The results were adjusted

for the radioactive decay of ^{18}F . The physiological distribution was calculated and expressed in terms of the percentage of administered dose found in each of the selected organs (%ID) or per gram of tissues/organ (%ID/g) with suitable standards of the injected dose.

The pharmacokinetic study was also conducted using non-radioactive reference standard of [^{18}F]SYN2 after a single i.v. administration at a dose of 2 mg/kg in rats. Blood samples of about 0.5 ml were collected in K₃-EDTA tubes at pre-dose time and 4 min, 15 min, 30 min, 60 min, 4 h, and 24 h after injection (three rats were used at each time point, each rat was bled twice). Blood samples were then centrifuged at approx. 3270 g at 5 ± 3 °C for 10 min to extract plasma, divided in two aliquots and analysed (54 plasma samples in total). The concentrations of SYN2 were determined according to a LC-MS/MS validated method according to the Guidance for Industry (FDA) and Guidance on Validation of Bioanalytical Methods (EMA).

Dosimetry

The pharmacokinetics data from ex vivo biodistribution studies in rats were extrapolated to humans using the simplest allometric scaling model to estimate an effective dose in mSv/MBq. The dose calculation was done using computer software for internal dose assessment OLINDA/EXM[®] (Version 1.1, copyright Vanderbilt University, 2007).

Toxicity

The potential health hazards resulting from exposure to intravenous administration of [^{18}F]SYN1 and [^{18}F]SYN2 were investigated. Extended single dose toxicity study after administration of 2 mg/kg b.w. of either test item (non-radioactive reference standards, SYN1 or SYN2) in a solution of 0.9% NaCl or only 0.9% NaCl into 30 males and 30 females of Wistar rats was investigated. The rats were euthanized 24 h ($n=40$) and 14 days ($n=20$) post-administration. Throughout the experiment, the animals' behaviour was observed and their weight recorded. The overview of animal groups used in the study is presented in Table 2.

Pharmacodynamics

The possibility of pharmacological interactions of SYN2 was assessed in vitro in radioligand binding assays on key pharmacological target classes including GPCRs, drug transporters, ion channels, nuclear receptors and enzymes (LeadProfilingScreen SafetyScreen, PP68, Panel of 68 receptors, Eurofins Panlabs, Inc.) [25]. There was only one SYN2 concentration of 1 μM used in the study. The significant response, which confirmed selective binding with target, was defined as $\geq 50\%$ inhibition or stimulation.

Table 2 Animal groups overview in the toxicity studies

Group	Number of animals		Administered item	Animal euthanasia
	males	females		
Control	0–1	10	0.9% NaCl solution	24 h post-administration
	0–2	5		14 days post-administration
Treated	1	10	Test item solution in 0.9% NaCl at dose 2 mg/kg b.w.	24 h post-administration
	2	5		14 days post-administration

Metabolites

The metabolite profiling and characterization experiment of SYN2 molecule (in vitro MetID, Admescope) was conducted to evaluate potential metabolic pathways. In order to characterize the metabolites of SYN2, the compound was incubated in cryopreserved rat, dog and human hepatocytes. Prior to the incubation, the hepatocytes were thawed, suspended in Williams medium E and then centrifuged to receive a target density of about 1 million cells/ml. A SYN2 solution of 1 μ M was then added to the hepatocyte suspension and incubated at 37 °C for 0, 30 and 60 min. The incubations were stopped by the addition of acetonitrile, then frozen and centrifuged to remove precipitated proteins. Supernatants were then analysed with ultra-performance liquid chromatography (UPLC) and high-resolution mass spectrometry (HRMS).

Statistical analysis

The results of radiopharmaceutical uptake are presented as a percentage of the dose administered per gram of tissue (%ID/g) in the form of an average with standard deviation (%ID/g; mean \pm standard deviation (SD)). Where applicable, statistical analysis was performed with one-way analysis of variance (ANOVA) using GraphPad Prism software (GraphPad Software, La Jolla, CA, USA).

The results of toxicity studies conducted for SYN1 and SYN2 were analysed using Excel 2013 and STATISTICA 10.0.PL. The normality distribution was tested with Shapiro-Wilk test. For homogeneity of variance Brown-Forsythe test has been used. For normal distribution and homogeneous variances results, Student's t-test was used. In the absence of normal distribution, Mann-Whitney test was used. In the case of non-homogenous variance, Cochran-Cox test was used.

IC₅₀ values from pharmacodynamics assessment were determined by a non-linear, least squares regression analysis using MathIQ™ (ID Business Solutions Ltd., UK). Where inhibition constants (K_i) are presented, the K_i values were calculated using the equation of Cheng and

Prusoff [26] using the observed IC₅₀ of the tested compound, the concentration of radioligand employed in the assay, and the historical values for the K_D of the ligand (obtained experimentally at Eurofins Panlabs, Inc.). Where presented, the Hill coefficient (n_H), defining the slope of the competitive binding curve, was calculated using MathIQ™.

Compound Discoverer (CD) was used for data mining with manual confirmation for metabolite profiling and characterization.

All of the obtained results were considered statistically significant for $p < 0.05$.

Results

The sterile radiotracers solutions with radiochemical purity >95% were achieved. The ethanol content was not higher than 10% and residual solvents concentration was within the *Ph.Eur.* limits. The stability of the formulation within 8 h was confirmed.

MicroPET

The dynamic microPET data (Fig. 3) showed higher accumulation of [¹⁸F]SYN2 compared to [¹⁸F]SYN1 in the organs of interest: heart, liver and lungs. The uptake of [¹⁸F]SYN2 in the myocardium was stable and high, the SUV value was 4.0 at the beginning and slightly decreased in time reaching plateau at a value of 3.5 after 6 min. In comparison, [¹⁸F]SYN1 uptake was lower (SUV 3.0 at the beginning) and decreased in time (SUV 1.8 after 45 min). The accumulation in the liver was higher for [¹⁸F]SYN2 with slower elimination compared to [¹⁸F]SYN1, the SUV_{max} of 2.9 was reached around 4 min with decrease to 1.9 at 45 min for [¹⁸F]SYN2, whilst for [¹⁸F]SYN1 the SUV_{max} was 2.4 at 2 min decreased to 1.0, respectively). However, the distribution ratio between heart and liver was comparable for both radiotracers and was equal to 1.2–1.3 for the first 10 min. The radioactivity uptake and retention in the lungs were also higher for [¹⁸F]SYN2. Small intestine and bladder were clearly

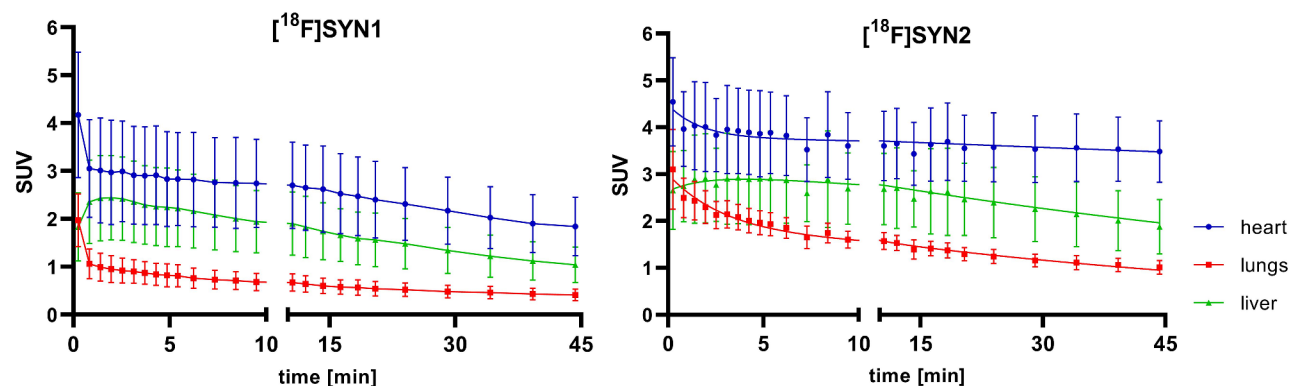


Fig. 3 MicroPET time-activity curves (TACs) of heart, lungs and liver for [¹⁸F]SYN1 and [¹⁸F]SYN2. Results are presented as mean standardized uptake value \pm standard error of measurement

visible 5 min post-injection (Figs. 4 and 5) and the SUV values increased in these organs with time.

Biodistribution and Pharmacokinetics

$[^{18}\text{F}]\text{SYN1}$ and $[^{18}\text{F}]\text{SYN2}$ generally showed a similar distribution. The critical organ for $[^{18}\text{F}]\text{SYN1}$ and $[^{18}\text{F}]\text{SYN2}$ was the intestine, with higher radioactivity uptake for $[^{18}\text{F}]\text{SYN1}$. The accumulation in the intestine increased over 15 min to 6 h from 22.0 ± 6.1 to $52.3 \pm 8.4\%$ ID for $[^{18}\text{F}]\text{SYN1}$ and from 17.1 ± 1.8 to $33.4 \pm 1.4\%$ ID for $[^{18}\text{F}]\text{SYN2}$. High and significant difference in compound accumulation was noted in the kidneys, for which $[^{18}\text{F}]\text{SYN2}$ accumulated at twice the rate of $[^{18}\text{F}]\text{SYN1}$ compound. For example, at 15 min the accumulation was 13.4 ± 4.0 and $5.4 \pm 1.5\%$ ID for $[^{18}\text{F}]\text{SYN2}$ and $[^{18}\text{F}]\text{SYN1}$, respectively, and at 6 h the value was 3.4 ± 0.4 and $0.5 \pm 0.1\%$ ID, respectively. All other organs examined retained only small amounts of test items, at level below 1% ID/g for $[^{18}\text{F}]\text{SYN1}$ and 2% ID/g for $[^{18}\text{F}]\text{SYN2}$.

Full data of tissue distribution are listed in Supplemental Tables 1–4.

The uptake of $[^{18}\text{F}]\text{SYN2}$ in the myocardium was stable and higher than 2.5% ID/g for up to 6 h, compared to $[^{18}\text{F}]\text{SYN1}$ which was between 2 and 1% ID/g up to 2 h, and then it dramatically decreased below 0.4% ID/g. Figure 6 shows comparative value uptake (%ID/g) in the heart as a target organ and in the lungs and the liver as critical organs during imaging.

Furthermore, we found that for $[^{18}\text{F}]\text{SYN2}$, the ratio of radioactivity accumulation in the heart to the liver and lungs was more favourable from an imaging point of view (Fig. 7). The most favourable and statistically significant ratios were observed after 2 h of radiotracer administration.

The blood pharmacokinetics of $[^{18}\text{F}]\text{SYN1}$ and $[^{18}\text{F}]\text{SYN2}$ as a one-phase and two-phase exponential decay model, respectively, are shown in Fig. 8. For $[^{18}\text{F}]\text{SYN2}$ the initial fast decrease mainly represents the

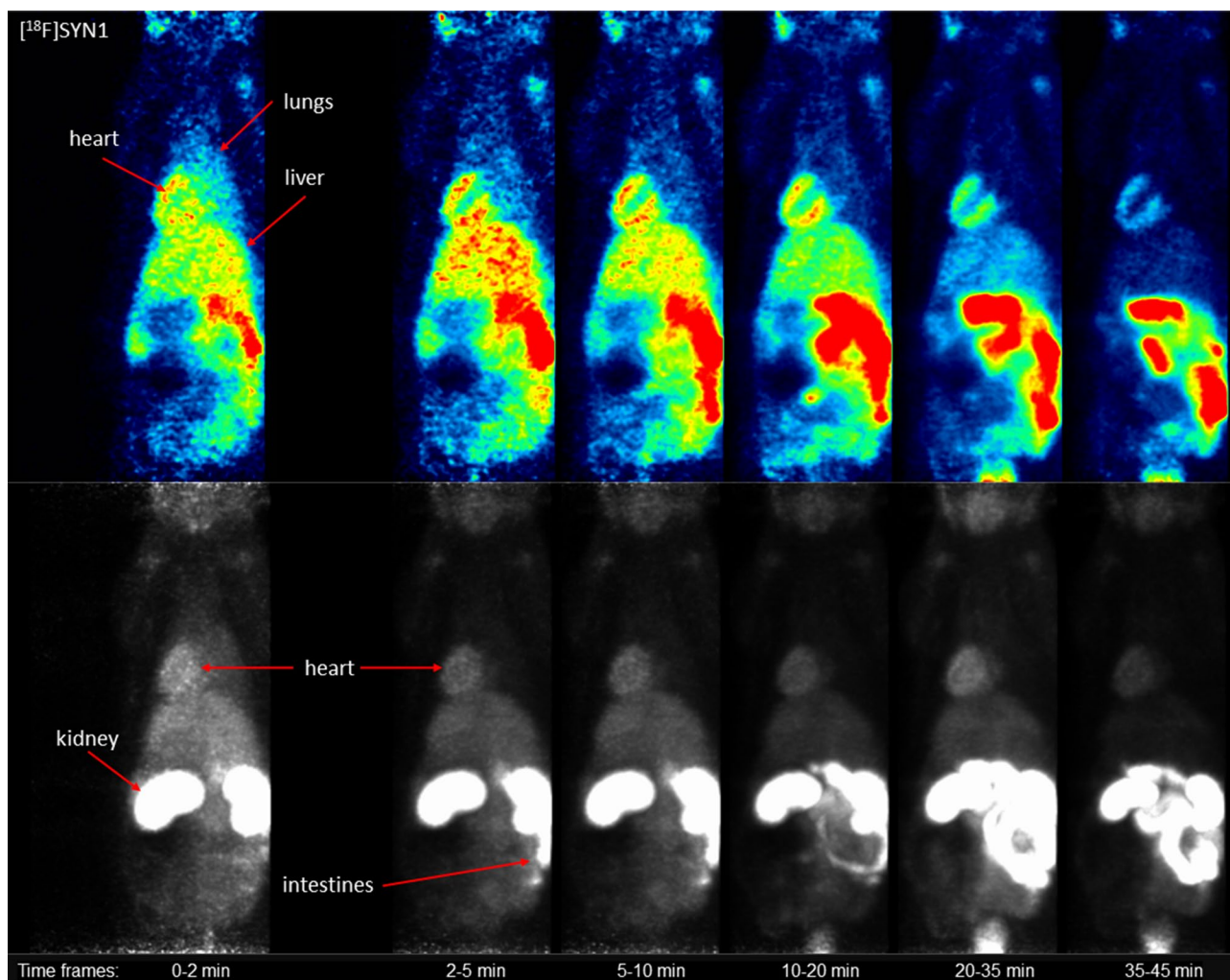


Fig. 4 Representative microPET images of $[^{18}\text{F}]\text{SYN1}$: slice (top) in the coronal plane and maximum intensity projection (bottom). Images represent the summation of time frames

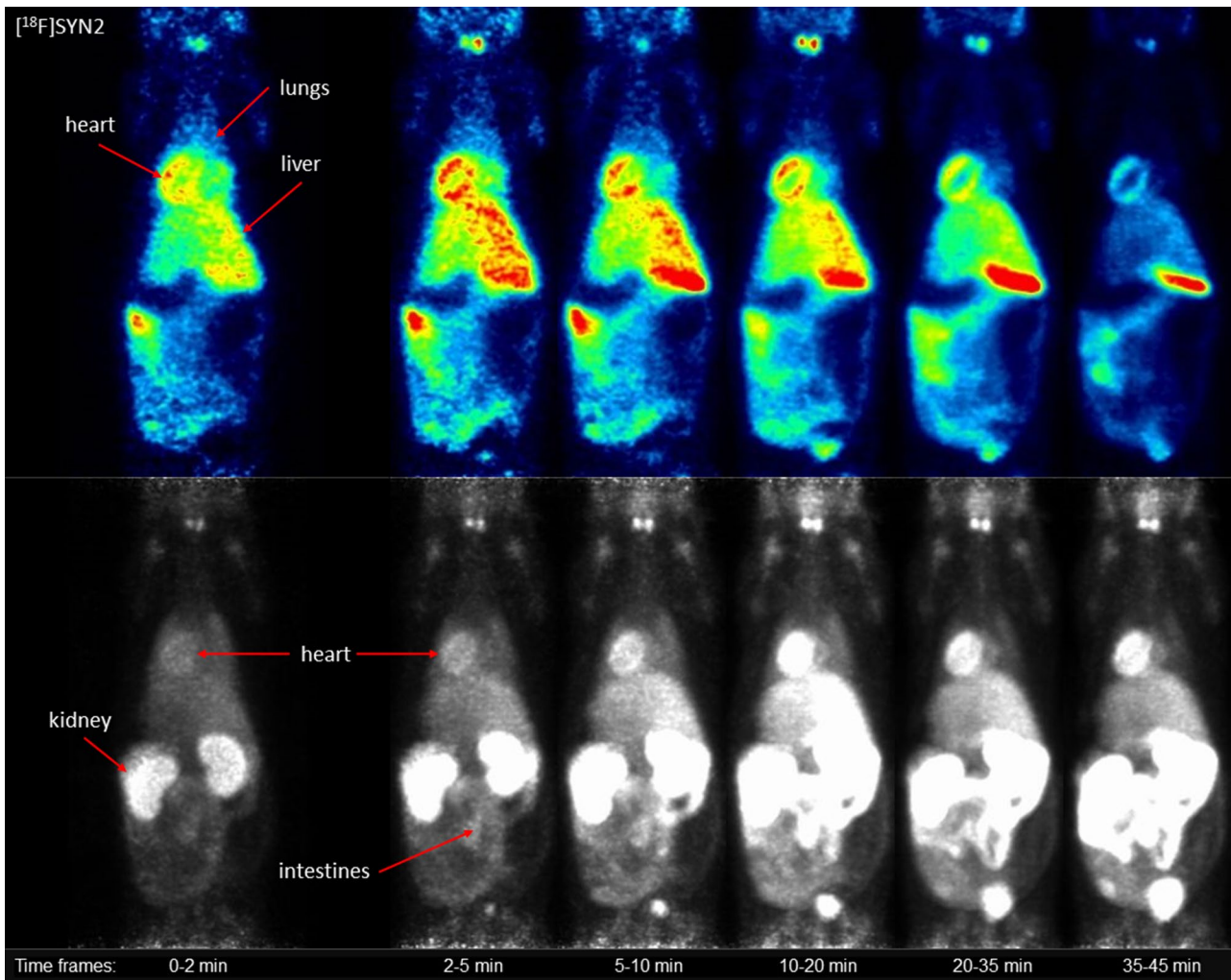


Fig. 5 Representative microPET images of $[^{18}\text{F}]\text{SYN2}$: slice (top) in the coronal plane and maximum intensity projection (bottom). Images represent the summation of time frames

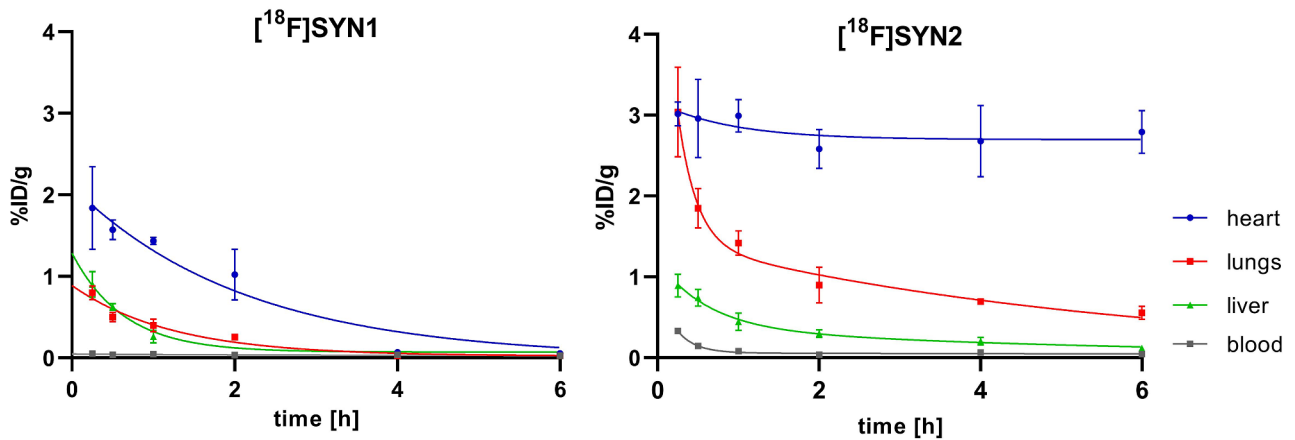


Fig. 6 Uptake of $[^{18}\text{F}]\text{SYN1}$ and $[^{18}\text{F}]\text{SYN2}$ in selected organs, ex vivo biodistribution study

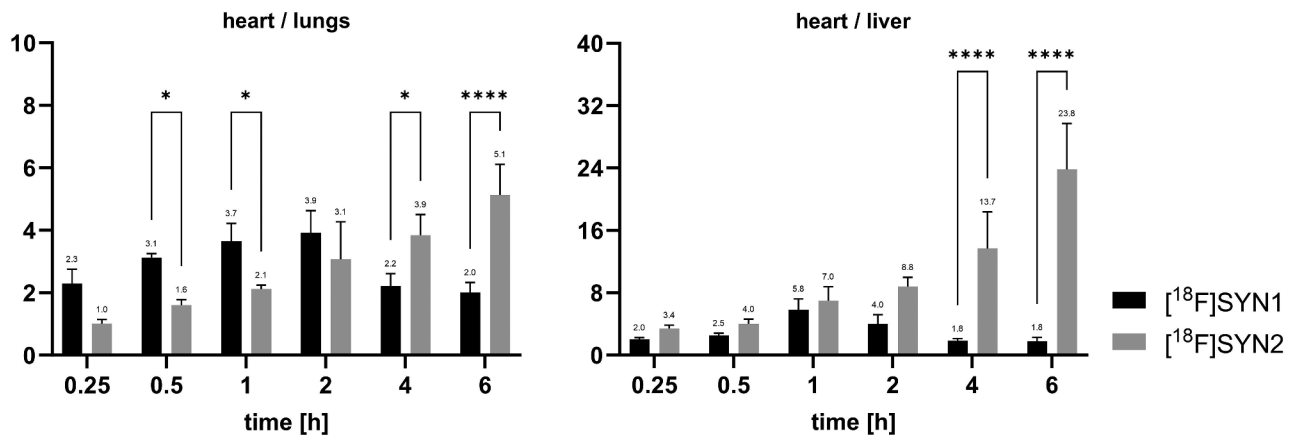


Fig. 7 Comparison of heart/lungs and heart/liver ratios between $[^{18}\text{F}]\text{SYN1}$ and $[^{18}\text{F}]\text{SYN2}$, calculation based on %ID/g

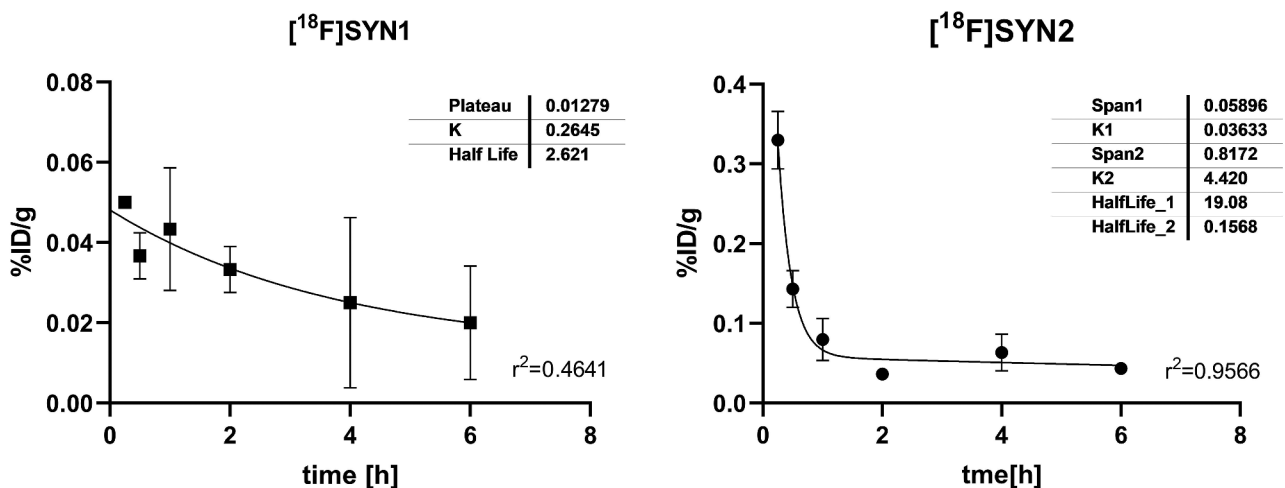


Fig. 8 Blood activity clearance. The fit of a one-phase and two-phase exponential model

Table 3 Pharmacokinetic parameters of SYN2 in the rat

T_{\max} (h)	C_{\max} (ng/mL)	T_{last} (h)	C_{last} (ng/mL)	AUC_t (h·ng/mL)	V_z (L/kg)	Cl (L/h/kg)	$T_{1/2\lambda z}$ (h)
0.07	368.67	1.00	8.95	73.75	0.99	2.59	0.26

T_{\max} – time to peak plasma concentration, C_{\max} – peak plasma concentration, T_{last} – time to last quantifiable plasma concentration, C_{last} – last quantifiable plasma concentration, AUC_t – area under the plasma concentration-time curve from time 0 to the time of the C_{last} , calculated by the linear trapezoidal linear/log rule, V_z – volume of distribution at the terminal phase, Cl – plasma clearance, $T_{1/2\lambda z}$ – terminal half-life

Table 4 Pharmacokinetic parameters for $[^{18}\text{F}]\text{SYN1}$ and $[^{18}\text{F}]\text{SYN2}$ in the rat

	T_{\max} [h]	C_{\max} [ng/mL]	AUC_t [h·ng/mL]	V_z [L/kg]	Cl [L/h/kg]	$T_{1/2}$ [h]*
$[^{18}\text{F}]\text{SYN1}$	0	40.99	73	3.12	0.037	57.8
$[^{18}\text{F}]\text{SYN2}$	0	76.39	421	1.43	0.012	79.9

$T_{1/2}$ – half-life calculated from Eq. $(0.693 \cdot V_z \cdot AUC)/\text{dose}$

equilibrium between the intravascular and extravascular components, and the second slower phase represents the metabolism.

It is worth mentioning that half-life parameters for $[^{18}\text{F}]\text{SYN1}$ and $[^{18}\text{F}]\text{SYN2}$ calculated from blood activity clearance differ from those presented in Table 3 which is most likely related to the administered dose. The

additional pharmacokinetic (PK) parameters for both radiolabelled compounds are presented in the Table 4.

The pharmacokinetics of $[^{18}\text{F}]\text{SYN2}$ was also measured using its non-radioactive reference standard SYN2. The tested item was quantifiable in plasma from the first sampling time point (4 min) down to 4 h. The plasma levels showed a rapid decay up to 1 h post injection. The elimination half-life was 0.26 h. The estimated plasma

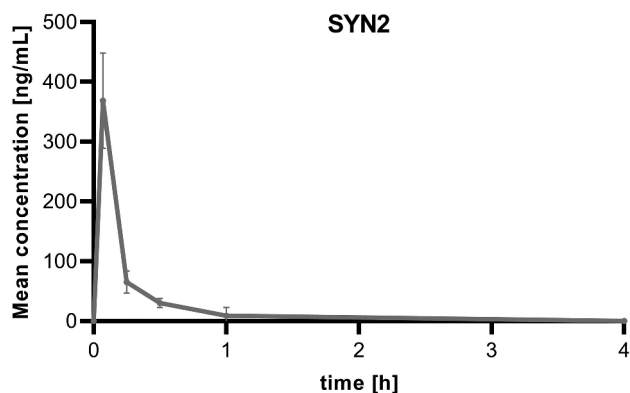


Fig. 9 Plasma concentration time profile for the unlabelled reference standard of $[^{18}\text{F}]\text{SYN2}$

Table 5 Toxicity study results

Conducted tests	SYN1*	SYN2*
<i>Clinical examinations</i>		
Mortality	-	-
Clinical observations	-	-
Body weight	-	-
<i>Clinical-chemical examinations</i>		
Haematological investigations	-	-
Biochemical investigations	+	+
Enzymatic investigations	+	+
<i>Post mortem examination</i>		
Gross examination	+	+
Weight of internal organs	-	+
Histopathological examinations	+	+

* "+" – statistically significant changes were observed between control and treated group

"-" – no statistically significant changes were observed

clearance was 2.59 L/h/kg. High total plasma clearance and low volume of distribution were obtained in the rats (Table 3; Fig. 9).

Safety

Toxicity

The objective of the toxicity study was to obtain information on health hazards resulting from a single exposure due to the intravenous administration of each of test item at dose of 2 mg/kg b.w., which is 1000-fold higher than the predicted maximum dose in humans.

The effects of each of test item on animals' body weight, clinical parameters as well as haematological, biochemical, enzymatic parameters, gross and histopathological lesions in tissues and internal organs were tested. Summary of collected data regarding the toxicity study of SYN1 and SYN2 is presented in Table 5 comparing if there were statistically significant changes observed between control and treated group.

Table 6 Estimates of absorbed doses (mSv/MBq) for $[^{18}\text{F}]\text{SYN1}$ and $[^{18}\text{F}]\text{SYN2}$ in human organs after extrapolation of biodistribution data in rats and absorbed doses for $[^{18}\text{F}]\text{flurpiridaz}$ derived from human studies [14]

Organs	Absorbed dose per administrated activity [mSv/MBq]		
	$[^{18}\text{F}]\text{SYN1}$	$[^{18}\text{F}]\text{SYN2}$	$[^{18}\text{F}]\text{Flurpiridaz}$
Adrenals	7.54E-03	8.06E-03	1.40E-02
Brain	2.00E-03	2.84E-03	1.10E-02
Breasts	5.17E-03	2.93E-03	1.00E-02
Gallbladder Wall	8.21E-03	8.01E-03	1.50E-02
Lower Large Intestine Wall	7.99E-03	1.18E-02	1.40E-02
Small Intestine	1.96E-02	1.84E-02	1.40E-02
Stomach Wall	7.88E-03	1.19E-02	2.40E-02
Upper Large Intestine Wall	9.18E-03	2.01E-02	1.40E-02
Heart Wall	1.39E-02	4.15E-02	3.90E-02
Kidneys	1.85E-02	7.04E-02	2.70E-02
Liver	7.63E-03	1.17E-02	1.50E-02
Lungs	6.95E-03	2.16E-02	1.20E-02
Muscle	6.17E-03	1.03E-02	1.20E-02
Ovaries	8.64E-03	7.10E-03	1.40E-02
Pancreas	1.11E-02	2.85E-02	1.50E-02
Red Marrow	6.08E-03	4.77E-03	1.50E-02
Osteogenic Cells	9.42E-03	4.02E-03	2.00E-02
Skin	4.79E-03	2.65E-03	9.00E-03
Spleen	6.09E-03	2.13E-02	1.30E-02
Testes	5.99E-03	4.97E-03	1.10E-02
Thymus	6.50E-03	5.48E-03	1.30E-02
Thyroid	6.18E-03	2.49E-02	1.40E-02
Urinary Bladder Wall	7.37E-03	5.29E-03	1.60E-02
Uterus	8.55E-03	6.27E-03	1.40E-02
Total Body	6.49E-03	7.67E-03	1.20E-02
Effective Dose Equivalent [mSv/MBq]	9.31E-03	1.71E-02	1.60E-02
Effective Dose [mSv/MBq]	7.14E-03	1.09E-02	1.50E-02

Dosimetry

This work estimated the human absorbed radiation dose based on a detailed description of activity organ distribution data for normal rats. After administration of $[^{18}\text{F}]\text{SYN1}$ and $[^{18}\text{F}]\text{SYN2}$, the animals were placed in holding cages which guaranteed their freedom of movement. Therefore, Table 6 compares estimated absorbed doses (mSv/MBq) in human organs for $[^{18}\text{F}]\text{SYN1}$ and $[^{18}\text{F}]\text{SYN2}$. Additionally, the obtained theoretical values for examined radiotracers were compared with $[^{18}\text{F}]\text{flurpiridaz}$ absorbed dose calculated in exercise stress subjects in humans (Table 6) [14].

The data in Table 6 shows that $[^{18}\text{F}]\text{SYN1}$ compound resulted in 34% less effective dose compared to $[^{18}\text{F}]\text{SYN2}$ and 52% as compared to $[^{18}\text{F}]\text{flurpiridaz}$. However, the dose absorbed in the heart wall was also clearly lower for $[^{18}\text{F}]\text{SYN1}$ (0.0139, 0.0415 and 0.0390 for $[^{18}\text{F}]\text{SYN1}$,

[^{18}F]SYN2 and [^{18}F]flurpiridaz, respectively), indicating a disadvantage of the [^{18}F]SYN1 compound.

The highest radiation-absorbed doses per unit-administered activity (mSv/MBq) of [^{18}F]SYN2 were calculated for kidneys (0.0704), heart wall (0.0415) and pancreas (0.0285), in contrast to [^{18}F]flurpiridaz for which the highest values were for heart wall (0.039), kidneys (0.027) and stomach wall (0.024). It's worth mentioning that the high value of the absorbed dose for [^{18}F]SYN2 in kidneys should not influence imaging quality of heart, which is related to the position of organs in the human body. However, obtained absorber dose for [^{18}F]SYN2 in kidneys is twice that of [$^{99\text{m}}\text{Tc}$]Tc-MIBI (0.036) [15], but at that level does not induce kidney toxicity.

The obtained preclinical data suggest that [^{18}F]SYN2 is a well-tolerated PET radiopharmaceutical with favourable radiation dosimetry profile and that is suitable for clinical cardiac imaging.

Pharmacodynamics

Radioligand binding assays showed significant responses ($\geq 50\%$ inhibition or stimulation) in three out of 68 assays: muscarinic acetylcholine M_1 receptor (58% inhibition), muscarinic M_2 acetylcholine receptor (68% inhibition) and potassium channel hERG (57% inhibition). The range of responses for the remaining 65 assays was from -12 to 43 (mean: 7.63, median: 4, IQR $[-1]$ – 13). Functional assays at several concentrations of SYN2 for IC_{50} or EC_{50} determination performed subsequently for muscarinic M_2 and hERG showed that SYN2 has an antagonistic effect on both targets with an IC_{50} about $1 \mu\text{M}$.

Metabolites

Twelve metabolites were identified in the study by analysis of high-resolution LC-MS/MS data and characterized in vitro in cryopreserved rat, dog and human hepatocytes (Supplemental Table 5). The products of reactions such as N-dealkylation, oxidation, acetylation and glucuronidation were identified and the fluorine atom was generally not detached. The metabolism of SYN2

in human hepatocytes was rather low in comparison to rat and dog (32% and 5% of the parent, respectively), the unchanged SYN2 was predominant after 60 min and was equal to 70% (Fig. 10). The major metabolite in dog cells was metabolite M1 and in rat cells metabolite M2. These metabolites appeared to be major metabolites in human hepatocytes with relative abundance of 19% and 8%, respectively at 60 min. In dog hepatocytes, the N-dealkylated metabolites M1, M2 and M3 were predominant at 60 min, respectively 58%, 53%, 46% of relative abundance. In rat cells the major metabolite was M2 (almost 7 times that of the parent at 60 min). The structures of M4, M5, M6, M7 and M8 were not fully elucidated due to very low contents, and generally may represent products of dealkylated/N-acetylated/oxidated forms of SYN2.

Discussion

We assessed biodistribution, pharmacokinetics, elimination and safety of [^{18}F]SYN1 and [^{18}F]SYN2, ^{18}F -labelled phenanthridine and acridine derivatives, respectively, candidate radiotracers for PET MPI. The further preclinical studies, pharmacodynamics and metabolism, were conducted only for [^{18}F]SYN2.

Myocardium was clearly visible in microPET for both radiotracers, however time-activity curves showed stable heart radioactivity uptake only for [^{18}F]SYN2 with high SUV values of 4.0–3.5 throughout the scan time (about 45 min). The microPET images suggested that both radiotracers were excreted via the biliary and urinary pathway. MicroPET also showed negligible skeletal activity, indicating that ^{18}F is not hydrolysed or released in the form of [^{18}F]fluoride ion in vivo for both compounds (Figs. 4 and 5).

The biodistribution studies demonstrated very similar results to microPET findings. They confirmed the higher than [^{18}F]SYN1 and sustained myocardial uptake of [^{18}F]SYN2 with values of about 3.0%ID/g within 1-hour post-injection and then 2.6–2.8%ID/g from 2 to 6 h. The uptake in the liver was also higher for [^{18}F]SYN2, and similarly to microPET results, the heart/liver ratio was also higher. The distribution profiles confirmed that both radiotracers were excreted via the biliary and urinary pathway (Supplemental Tables 1–4).

The biodistribution results of [^{18}F]SYN2 can be compared with other tracers for myocardial perfusion, like [^{18}F]flurpiridaz (former name ^{18}F -BMS-747158-02) and [$^{99\text{m}}\text{Tc}$]Tc-sestamibi. For example, at 1 h post-injection the accumulation in cardiac tissue was comparable with [^{18}F]flurpiridaz, 3.0 ± 0.2 vs. $3.3 \pm 0.3\%$ ID/g, respectively, and higher than [$^{99\text{m}}\text{Tc}$]Tc-sestamibi ($2.0 \pm 0.3\%$ ID/g). However, the heart/liver ratio was the highest for [^{18}F]SYN2, 7.0 ± 1.8 vs. 3.7 ± 0.2 and 2.4 ± 0.2 , respectively. The heart/lungs ratio was on the other hand the lowest for [^{18}F]SYN2, ratio of 2.1 ± 0.2 vs. 12.7 ± 1.4 and 5.9 ± 0.5 ,

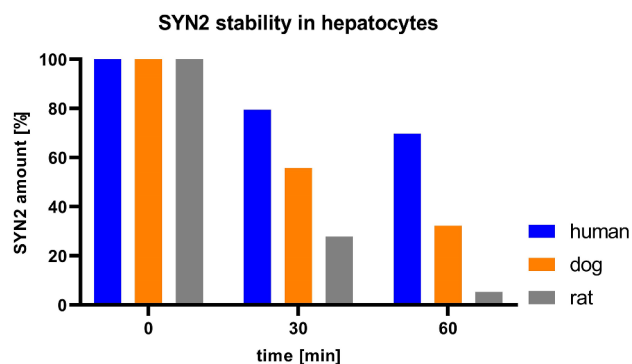


Fig. 10 Stability of SYN2 in human, dog and rat hepatocytes

respectively [27]. Furthermore, the heart/blood ratio was significantly higher for [^{18}F]SYN2 in comparison with [^{18}F]flurpiridaz (37 vs. 13) [28]. The observed differences between the biodistribution parameters of ^{18}F -labelled radiotracer, [^{18}F]SYN2 and [^{18}F]flurpiridaz, are not significant enough to draw conclusion, which tracer is the best for myocardial perfusion imaging, however both has advantage over [$^{99\text{m}}\text{Tc}$]Tc-sestamibi. Therefore, further clinical studies are warranted.

The approximated estimation of [^{18}F]SYN2 dosimetry in humans showed that the organ receiving the highest estimated absorbed dose were the kidneys at 0.070 mSv/MBq, followed by the heart wall at 0.042 mSv/MBq (Table 6). The value for heart wall is comparable to [^{18}F]flurpiridaz, the new cardiac perfusion agent now in phase III clinical trials (0.027 mSv/MBq and 0.039 mSv/MBq, respectively) [14]. The estimation for [^{18}F]SYN1, the second tested compound, showed that the small intestine received the highest estimated absorbed dose at 0.020 mSv/MBq, followed by the kidney at 0.019 mSv/MBq and heart wall with much lower value compared to [^{18}F]SYN2 and [^{18}F]flurpiridaz at 0.014 mSv/MBq (Table 6). The effective dose of [^{18}F]SYN1 was the lowest, followed by [^{18}F]SYN2 and then [^{18}F]flurpiridaz – 0.0072 mSv/MBq vs. 0.0109 mSv/MBq vs. 0.0150 mSv/MBq, respectively [14]. For comparison, effective doses for ^{82}Rb and [^{13}N]ammonia, short lived radiotracer, are much lower, 0.0011 mSv/MBq and 0.002 mSv/MBq, respectively [15, 16]. The in-house data of estimated dosimetry of the ^{18}F -labelled compounds presented in this paper are derived from allometrically scaled results from rat studies to humans. This is an important limitation and may result in discrepancies from the dosimetry determined in direct human studies. Such studies are planned.

SYN1 and SYN2 were well-tolerated and only slight abnormalities were reported in the toxicological study. The minor biochemical abnormalities were within the normal limits for Wistar rats [29]. Minimally increased incidence of basophilic tubules in the kidneys of male rats (without other renal changes) might have been the result of spontaneously occurring chronic progressive nephropathy, one of the most common spontaneous diseases in rats correlated with age [30]. Hepatocyte karyomegaly and foci of single hepatocyte necrosis are a normal incidental finding in the rats and may occur spontaneously with age [31]. In conclusion, the histopathological changes found in all study groups were background findings and although they might have been related to SYN1 or SYN2 administration, the dose level of 2 mg/kg b.w. is considered to be “no observed adverse effect level” (NOAEL).

The high and stable uptake of the [^{18}F]SYN2 in the heart muscle together with good heart/liver distribution ratio and low toxicity make this radiotracer suitable for

the heart muscle imaging. Therefore, further preclinical studies were conducted only with the [^{18}F]SYN2.

The possible pharmacological interactions of SYN2 were tested and significant inhibition was observed for 3 out of 68 targets at a concentration of 1 μM – muscarinic acetylcholine receptors M_1 and M_2 as well as hERG. The determined values indicate that SYN2 show high affinity to hERG receptors and moderate to muscarinic receptors [32]. The muscarinic acetylcholine receptors are multifunctional, they are responsible for regulating heart rate, smooth muscle contraction, glandular secretion and many fundamental functions of the central nervous system [33], while hERG plays an important role in electrical activity in the heart [34]. The affinity of acridine derivatives to hERG receptors was already confirmed in the range of 0.2–18 μM [35]. The structure that has positively charged nitrogen atom and hydrophobic aromatic ring system can be deduced as a potential hERG blocker using QSAR strategy. The results of analysing different database highlighted that hERG inhibitors tend to have a larger molecular weight, higher hydrophobicity, more cations and less basic substituents [35]. Similar conclusion can be applied to muscarinic receptors, e.g. the tacrine, acridine derivative, is the known antagonist [36].

Despite the wide abundance of mentioned targets in the human body (including heart) any interactions of SYN2 are considered unlikely, as it reached low plasma concentrations [37–40]. We demonstrated in normal Wistar rats that SYN2 reached C_{max} of 0.19 μM after i.v., injection of 2 mg/kg with a half-life of 0.26 h. After injection of a proposed maximum limit dose of 100 μg (2 $\mu\text{g}/\text{kg}$ for a 50-kg patient), we expect C_{max} of 1.1 nM after body surface area correction, which is unreliable to lead to any measurable biological effects.

The metabolic profiles in human, dog and rat hepatocytes were compared to evaluate potential metabolism pathways. Firstly, the drug product usually undergoes reaction of functionalization, very frequent to be more polar. The metabolites found in dog, rat and human hepatocytes suggest that SYN2 is mainly oxidatively N-dealkylated in a subsequent mode forming M1 and M2 metabolites. In addition, in dog and rat hepatocytes the M3 metabolite was observed as well. Only the structures of M1, M2 and M3 were confirmed by MS fragmentation spectra to high content. However, it seems that hydroxylation can occur as well as metabolites M5, M6 were detected [41], though the forming of N-oxide cannot be excluded. Secondly, metabolites are usually coupled with an endogenous molecule undergoing acetylation or (N, O)-glucuronidation reaction. Metabolites M7, M8 are N-acetylation products similarly to proflavine [42]. The product of the last reaction is only observed in rat and dog hepatocytes presumably to slower metabolism in human cells. The gathered data indicated that

main metabolism of SYN2 proceeded via oxidative N-dealkylation(s) followed by acetylation yielded polar metabolites that can be excreted in urine and/or bile. The other pathway seen in dog and rat hepatocytes via hydroxylation and O-glucuronidation appear to be of lower significance. Similarly, the dealkylation at N-acridine atom, followed by cleavage of fluorine atom is of lower significance due to the fact that quaternary amines are more stable than tertiary or secondary amines toward N-dealkylation.

Conclusions

[¹⁸F]SYN2 showed favourable pharmacodynamic and pharmacokinetic profile in normal Wistar rats. The tracer, with its rapid plasma clearance, high and stable uptake in the myocardium and favourable heart to lung ratio, allowed for a clear visualization of the heart in microPET. [¹⁸F]SYN2 was safe, well-tolerated and showed moderate radiation exposure comparable with other MPI PET tracers. Promising results of preclinical evaluation of [¹⁸F]SYN2 encourage its further exploration in clinical studies.

Abbreviations

[¹⁸ F]SYN1	¹⁸ F-labelled derivative of ethidium bromide
[¹⁸ F]SYN2	¹⁸ F-labelled derivative of acridine orange
%ID	Percentage of injected dose per organ
%ID/g	Percentage of injected dose per gram of tissue
API	Active pharmaceutical ingredient
AUCT	Area under the plasma concentration curve from time 0 to the time of the C _{last} calculated by the linear trapezoidal linear/log rule
BODIPY	Boron-dipyrromethene
CAD	Coronary artery disease
Cl	Plasma clearance
C _{last}	last quantifiable plasma concentration
C _{max}	Peak plasma concentration
CPN	Chronic Progressive Nephropathy
DCM	Dichloromethane
EMA	European Medicines Agency
EthBr	Ethidium bromide
FDA	Food and Drug Administration
HRMS	High-resolution mass spectrometry
IC ₅₀	Half maximal inhibitory concentration
ICA	Invasive Coronary Angiography
IHD	Ischemic heart disease
MBF	Myocardial blood flow quantification
MPI	Myocardial perfusion imaging
NOA	N-nonyl acridine orange
NOAEL	No observed adverse effect level
PCM	Progressive Cardiomyopathy
PET	Positron emission tomography
RCP	Radiochemical purity
SD	Standard deviation
SPECT	Single photon emission computed tomography
SYN1	Non-radioactive reference standard of [¹⁸ F]SYN1
SYN2	Non-radioactive reference standard of [¹⁸ F]SYN2
T _{1/2z}	Terminal half-life
T _{last}	Time to last quantifiable plasma concentration
T _{max}	Time to peak plasma concentration
UPLC	Ultra-performance liquid chromatography
WHO	World Health Organization
V _z	Volume of distribution at the terminal phase

Supplementary Information

The online version contains supplementary material available at <https://doi.org/10.1186/s13550-024-01122-5>.

Supplementary Material 1

Acknowledgements

We thank Dr. Zbigniew Rogulski and Łukasz Cheda (University of Warsaw) for conducting the microPET imaging and analysis.

Author contributions

Conceptualization, S.K., K.G., L.S., U.K., P.G.; methodology, U.K., P.G., S.K., J.W., J.T.; writing—original draft preparation, S.K., K.G., L.S., E.W.P., M.D., U.K., P.G.; writing—review and editing, S.K., K.G., L.S., U.K., P.G., E.W.P., J.K., M.M., C.K., P.K., J.W.; organic synthesis, L.S.; compounds analysis, L.S., S.K., K.G., K.Ł.; radiosynthesis, S.K., L.S., K.G.; in vivo studies U.K.; project management, P.K., C.K., J.T., J.W. All authors have given approval to the final version of the manuscript.

Funding

The study was supported by National Centre for Research and Development, Poland, grant no. POIR.01.01.01-00-0089/15.

Data availability

The datasets used and/or analyzed during the current study are available from the corresponding author on reasonable request.

Declarations

Ethical approval

All methods were carried out in accordance with relevant guidelines and regulations. The animal procedures were approved by Animal Ethics Committees: the microPET and ex vivo biodistribution protocols were approved by the 1st Local Animal Ethics Committee in Warsaw (authorization 069/2016, approval date 15 June 2016, with further changes 445/2017 and authorization 400/2017, approval date 21 November 2017, respectively), the toxicity studies were approved by Local Animal Ethical Committee in Katowice, Poland (authorizations 45/2018 and 107/2018, approval dates 16 May and 16 November 2018) and pharmacokinetic profile with SYN2 was carried out based on authorization no. PROEX 211/10 (approval date 12.09.2019) issued by Spanish General Director of Agriculture, Livestock and Food. The study was carried out in compliance with the ARRIVE guidelines.

Consent to participate

No human participants or human data was involved in the study. Hepatocytes of human (50-donor, Lot no. HQE, X008005), dog (Male Beagle dog, Lot no. UXH, M00205) and rat (Male Wistar rat, Lot no. ATI, M00025) were purchased from BioreclamationIVT (Brussels, Belgium).

Consent for publication

Not applicable.

Competing interests

J.K. and M.D. are advisors and received the consultant honoraria from Synektik SA. The other authors have no relevant financial or non-financial interests to disclose.

Received: 5 April 2024 / Accepted: 20 June 2024

Published online: 08 July 2024

References

1. Werner RA, Chen X, Rowe SP, Lapa C, Javadi MS, Higuchi T. Recent paradigm shifts in molecular cardiac imaging—establishing precision cardiology through novel ¹⁸F-labeled PET radiotracers. *Trends Cardiovasc Med*. 2020;30:11–9. <https://doi.org/10.1016/j.tcm.2019.02.007>.
2. Knuuti J, Wijns W, Saraste A, Capodanno D, Barbato E, Funck-Brentano C, et al. 2019 ESC guidelines for the diagnosis and management of chronic coronary

- syndromes. *Eur Heart J*. 2020;14:407–77. <https://doi.org/10.1093/eurheartj/ehz425>.
3. Singh V, Di Carli MF. SPECT Versus PET myocardial perfusion imaging in patients with equivocal CT. *Curr Cardiol Rep*. 2020;22:43. <https://doi.org/10.1007/s11886-020-01287-0>.
 4. Li J, Lu J, Zhou Y. Mitochondrial-targeted molecular imaging in cardiac disease. *Biomed Res Int*. 2017;2017:5246853. <https://doi.org/10.1155/2017/5246853>.
 5. Srivastava AV, Ananthasubramaniam K. Guiding coronary revascularization using PET stress myocardial perfusion imaging: the proof is in the pudding. *J Nucl Cardiol*. 2017;24:975–9. <https://doi.org/10.1007/s12350-016-0479-2>.
 6. Chen K, Miller EJ, Sadeghi MM. PET-Based imaging of Ischemic Heart Disease. *PET Clin*. 2019;14:211–21. <https://doi.org/10.1016/j.cpet.2018.12.003>.
 7. Mou T, Zhang X. Research progress on ¹⁸F-labeled agents for imaging of myocardial perfusion with positron emission tomography. *Molecules*. 2017;22:562. <https://doi.org/10.3390/molecules22040562>.
 8. Klein R, Celiker-Guler E, Rotstein BH, deKemp RA. PET and SPECT Tracers for Myocardial Perfusion Imaging. *Semin Nucl Med*. 2020;50:208–18. <https://doi.org/10.1053/j.semnuclmed.2020.02.016>.
 9. Medicines Agency E, Rubidium Chloride. Jan RB-82: List of Nationally Authorised Medicinal Products - PSUSA/00010806/202110. https://www.ema.europa.eu/en/documents/psusa/rubidium-82rb-chloride-list-nationally-authorised-medicinal-products-psusa00010806202110_en.pdf. Accessed 18 2024.
 10. Zhao Z, Yu Q, Mou T, Liu C, Yang W, Fang W, et al. Highly efficient one-pot labeling of new phosphonium cations with fluorine-18 as potential PET agents for myocardial perfusion imaging. *Mol Pharm*. 2014;11:3823–31. <https://doi.org/10.1021/mp500216g>.
 11. Zeng H, Wu X, Song F, Xu C, Liu H, Liu W. Synthesis and evaluation of [¹⁸F]-fluoromethyl triphenylphosphonium cation as a novel mitochondria-specific positron emission tomography tracer. *Eur J Med Chem*. 2016;118:90–7. <https://doi.org/10.1016/j.ejmech.2016.04.036>.
 12. Bartholomä MD, Zhang S, Akurathi V, Pacak CA, Dunning P, Fahey FH, et al. ¹⁸F-labeled rhodamines as potential myocardial perfusion agents: comparison of pharmacokinetic properties of several rhodamines. *Nucl Med Biol*. 2015;42:796–803. <https://doi.org/10.1016/j.nuclmedbio.2015.06.008>.
 13. Maddahi J, Agostini D, Bateman TM, Bax JJ, Beanlands RSB, Berman DS, et al. Flurpiridaz F-18 PET myocardial perfusion imaging in patients with suspected coronary artery disease. *J Am Coll Cardiol*. 2023;82:1598–610. <https://doi.org/10.1016/j.jacc.2023.08.016>.
 14. Maddahi J, Bengel F, Czernin J, Crane P, Dahlbom M, Schelbert H, et al. Dosimetry, biodistribution, and safety of flurpiridaz F 18 in healthy subjects undergoing rest and exercise or pharmacological stress PET myocardial perfusion imaging. *J Nuclear Cardiol*. 2019;26:2018–30. <https://doi.org/10.1007/s12350-018-01484-z>.
 15. Mattsson S, Johansson L, Leide Svegborn S, Liniecki J, Noßke D, Riklund KÅ et al. ICRP, 2015. Radiation Dose to Patients from Radiopharmaceuticals: a Compendium of Current Information Related to Frequently Used Substances. ICRP Publication 128. Ann. ICRP 44(2S). Clement, C. H.; Hamada, N., Eds., SAGE, 2015.
 16. ICRP. 1998. Radiation Dose to Patients from Radiopharmaceuticals (Addendum to ICRP Publication 53). ICRP Publication 80. Ann. ICRP 28 (3). Valentín J, Ed., Pergamon, 1998, 113.
 17. Hyafil F, Gimelli A, Slart RHJA, Georgoulas P, Rischpler C, Lubberink M, et al. EANM procedural guidelines for myocardial perfusion scintigraphy using cardiac-centered gamma cameras. *Eur J Hybrid Imaging*. 2019;3:11. <https://doi.org/10.1186/s41824-019-0058-2>.
 18. Scigrà R, Lubberink M, Hyafil F, Saraste A, Riemer, Slart HJA, et al. EANM procedural guidelines for PET/CT quantitative myocardial perfusion imaging. *Eur J Nucl Med Mol Imaging*. 2021;48:1040–69. <https://doi.org/10.1007/s00259-020-05046-9>.
 19. Xu J, Cai F, Geng C, Wang Z, Tang X. Diagnostic performance of CMR, SPECT, and PET imaging for the identification of coronary artery disease: a Meta-analysis. *Front Cardiovasc Med*. 2021;8:621389. <https://doi.org/10.3389/fcvm.2021.621389>.
 20. Sogbein OO, Pelletier-Galarneau M, Schindler TH, Wei L, Wells RG, Ruddy TD. New SPECT and PET radiopharmaceuticals for imaging cardiovascular disease. *Biomed Res Int*. 2014;2014:942960. <https://doi.org/10.1155/2014/942960>.
 21. Chansaenpak K, Wang H, Wang M, Giglio B, Ma X, Yuan H, et al. Synthesis and evaluation of [¹⁸F]-Ammonium BODIPY dyes as potential Positron Emission Tomography agents for myocardial perfusion imaging. *Chemistry*. 2016;22:12122–9. <https://doi.org/10.1002/chem.201601972>.
 22. Petit J-M, Maftah A, Ratinaud M, -H, Julien R. 10 N-Nonyl acridine orange interacts with cardiolipin and allows the quantification of this phospholipid in isolated mitochondria. *Eur J Biochem*. 1992;209:267–73. <https://doi.org/10.1111/j.1432-1033.1992.tb17285.x>.
 23. Towpik J, Krajewski S, Steczek L, Wlostowska JA, Radiolabelled Compound. Of Quaternary Ammonium Salt Of A Polycyclic Aromatic Amine, The Use Of The Radiolabelled Compound In A Diagnostic Method Of Positron Emission Tomography, And A Pharmaceutical Composition Containing The Radiolabelled Compound Of Quaternary Ammonium Salt Of A Polycyclic Aromatic Amine. EP3814325B1, September 4 2019. <https://worldwide.espacenet.com/patent/search/family/068208328/publication/EP3814325B1?q=EP3814325B1>. Accessed 20 Jul 2023.
 24. du Sert NP, Ahluwalia A, Alam S, Avey MT, Baker M, Browne WJ, et al. Reporting animal research: explanation and elaboration for the arrive guidelines 2.0. *PLoS Biol*. 2020;18:e3000411. <https://doi.org/10.1371/journal.pbio.3000411>.
 25. LeadProfilingScreen SafetyScreen Panel - TW. <https://www.eurofindsdiscovery.com/catalog/leadprofilingscreen-safetyscreen-panel-tw/PP68>. Accessed 13 Nov 2023.
 26. Yung-Chi C, Prusoff WH. Relationship between the inhibition constant (KI) and the concentration of inhibitor which causes 50 per cent inhibition (I50) of an enzymatic reaction. *Biochem Pharmacol*. 1973;22:3099–108. [https://doi.org/10.1016/0006-2952\(73\)90196-2](https://doi.org/10.1016/0006-2952(73)90196-2).
 27. Yu M, Nekolla SG, Schwaiger M, Robinson SP. The next generation of cardiac positron emission tomography imaging agents: discovery of flurpiridaz F-18 for detection of coronary disease. *Semin Nucl Med*. 2011;41:305–13. <https://doi.org/10.1053/j.semnuclmed.2011.02.004>.
 28. Huisman MC, Higuchi T, Reder S, Nekolla SG, PoethkoT, Wester H-J, et al. Initial characterization of an ¹⁸F-labeled myocardial perfusion tracer. *J Nucl Med*. 2008;49:630–6. <https://doi.org/10.2967/jnumed.107.044727>.
 29. Clinical laboratory parameters for CrI. Wi(Han) rats. https://hero.epa.gov/hero/index.cfm/reference/details/reference_id/1873773. Accessed 20 Jul 2023.
 30. Frazier KS, Seely JC, Hard GC, Betton G, Burnett R, Nakatsui S, et al. Proliferative and nonproliferative lesions of the rat and mouse urinary system. *Toxicol Pathol*. 2012;40:S14–86. <https://doi.org/10.1177/0192623312438736>.
 31. Thoolen B, Maronpot RR, Harada T, Nyska A, Rousseaux C, Nolte T, et al. Proliferative and nonproliferative lesions of the rat and mouse hepatobiliary system. *Toxicol Pathol*. 2010;38:S3–81. <https://doi.org/10.1177/0192623310386499>.
 32. Krippendorff BF, Lienau P, Reichel A, Huisinga W. Optimizing classification of drug-drug interaction potential for CYP450 isoenzyme inhibition assays in early drug discovery. *J Biomol Screen*. 2007;12:92–9. <https://doi.org/10.1177/1087057106295897>.
 33. Kruse AC, Kobilka BK, Gautam D, Sexton PM, Christopoulos A, Wess J. Muscarinic acetylcholine receptors: novel opportunities for drug development. *Nat Rev Drug Discov*. 2014;13:549–60. <https://doi.org/10.1038/nrd4295>.
 34. Garrido A, Lepailleur A, Mignani SM, Dallemagne P, Rochais C. hERG toxicity assessment: useful guidelines for drug design. *Eur J Med Chem*. 2020;195:112290. <https://doi.org/10.1016/j.ejmech.2020.112290>.
 35. Iachettini S, Stevens MFG, Frigerio M, Hummersone MG, Hutchinson I, Garner TP, et al. On and off-target effects of telomere uncapping G-quadruplex selective ligands based on pentacyclic acridinium salts. *J Exp Clin Cancer Res*. 2013;32:68. <https://doi.org/10.1186/1756-9966-32-68>.
 36. Becerra MA, Herrera MD, Marhuenda E. Action of tacrine on muscarinic receptors in rat intestinal smooth muscle. *J Auton Pharmacol*. 2001;21:113–9. <https://doi.org/10.1046/j.1365-2680.2001.00213.x>.
 37. Jiang S, Li Y, Zhang C, Zhao Y, Bu G, Xu H, et al. M1 muscarinic acetylcholine receptor in Alzheimer's disease. *Neurosci Bull*. 2014;30:295–307. <https://doi.org/10.1007/s12264-013-1406-z>.
 38. Miyakawa T, Yamada M, Duttaroy A, Rgen Wess J. Hyperactivity and Intact Hippocampus-Dependent Learning in mice lacking the M₁ muscarinic acetylcholine receptor. 2001;21:5239–50. <https://doi.org/10.1523/JNEUROSCI.121-14-05239.2001>.
 39. Lebois EP, Bridges TM, Lewis LM, Dawson ES, Xiang Z, et al. Discovery and characterization of novel subtype-selective allosteric agonists for the investigation of M1 receptor function in the central nervous system. *ACS Chem Neurosci*. 2010;1:104–21. <https://doi.org/10.1021/cn900003h>.
 40. Witchel HJ. Drug-induced hERG block and long QT syndrome. *Cardiovasc Ther*. 2011;29:251–9. <https://doi.org/10.1111/j.1755-5922.2010.00154.x>.
 41. Spaldin V, Madden S, Pool WF, Woolf TF, Park BK. The effect of enzyme inhibition on the metabolism and activation of tacrine by human liver microsomes.

Br J Clin Pharmacol. 1994;38:15–22. <https://doi.org/10.1111/j.1365-2125.1994.tb04316.x>.

42. Plakas SM, El Said KR, Bencsath FA, Musser SM, Hayton WL. Pharmacokinetics, tissue distribution and metabolism of acriflavine and proflavine in the channel catfish (*Ictalurus punctatus*). *Xenobiotica*. 1998;28:605–16. <https://doi.org/10.1080/004982598239353>.

Publisher's Note

Springer Nature remains neutral with regard to jurisdictional claims in published maps and institutional affiliations.